THE PHOTOGRAMMETRIC RECORD

The Photogrammetric Record 28(144): 416–435 (December 2013)
DOI: 10.1111/phor.12039

DIGITAL ELEVATION QUALITY DERIVED FROM MEDIUM-FORMAT DIGITAL CAMERAS

P. T. Y. Shih (tyshih@mail.nctu.edu.tw)
J. Y. Wu (elvislikebear@gmail.com)
T. A. Teo (tateo@mail.nctu.edu.tw)
J. C. Tsai (ken_4_26@hotmail.com)
National ChiaoTung University, Hsinchu, Taiwan

Abstract

Medium-format digital cameras are a useful tool in airborne lidar missions to produce digital ortho-images. This study investigates the quality of digital elevation models (DEMs) and digital surface models (DSMs) derived from such cameras. An image-matching strategy is used to produce height information from highly overlapping images and the quality of the derived height information is analysed using synchronous lidar point clouds as the reference data. The evaluation focused on various types of land cover and DEM generation methods. The RMSE between lidar and image-derived height information for two datasets was 0·054% and 0·027% of the flying height in flat, bare-earth areas, but studies with manually edited vegetated areas using stereo photogrammetry revealed high uncertainties, especially in steep terrain.

Keywords: automated matching, digital elevation model, image matching, lidar, medium-format cameras

Introduction

Although an increasing number of airborne lidar units are being implemented operationally, photogrammetry remains an effective methodology for producing digital elevation models (DEMs). When favourable conditions are met, photogrammetry can provide a more economical way to produce such models. Although airborne lidar provides an effective means for collecting informative data, such as the terrain surface and structures (Höhle, 2013), optical images, such as conventional aerial photographs, remain in high demand because of their abundant planimetric information, which can provide detailed information of features such as buildings and roads. Therefore, nearly all airborne lidar units currently in operation are equipped with medium-format digital cameras.

Petrie and Walker (2007) grouped digital cameras into three categories based on image size: small format (fewer than 16 megapixels), medium format (16 to 50 megapixels) and large format (more than 50 megapixels). Medium-format cameras include the Applanix DSS, Rollei AIC and DuncanTech DT4000. Large-format camera producers currently also manufacture medium-format digital cameras; Leica produces the RCD 30 and RCD 105, Z/I

manufactures the RMK D and Vexcel markets the UltraCam L and its successor, the UltraCam LP. The justification for this practice may be that such cameras can serve as an add-on to airborne lidar units.

The main advantages of medium-format digital cameras include low cost, flexibility because of low weight and interchangeable lenses, as well as easy and fast post-processing of single-head camera images (Habib et al., 2007; Grenzdörffer, 2010). Medium-format digital cameras are typically equipped with interchangeable lenses with focal lengths from 35 to 210 mm. These various lenses allow diverse types of missions to be flown at different altitudes to maintain the desired resolution or the predefined strip width, which may be determined by other sensors. Medium-format digital cameras have particular problems related to camera calibration and stability analysis (Brown, 1966; Habib and Morgan, 2005; Rieke-Zapp, 2010). Usually, the geometric calibration accuracy of medium-format digital cameras is slightly lower than that of large-format digital camera systems such as the DMC and UltraCam D. Therefore, camera calibration and the stability of medium-format digital cameras are crucial.

A large proportion of medium-format digital cameras are used as a sub-system of integrated airborne data acquisition platforms consisting of lidar combined with imaging components and Global Positioning System (GPS)/internal sensors for direct platform orientation. The role of medium-format digital cameras is gaining importance in photogrammetric missions. It is evident that the disadvantages of one system can be compensated for by the advantages of another system (Baltsavias, 1999). However, the synergic characteristics of both systems can be thoroughly exploited only after ensuring that both datasets are georeferenced in relation to the same reference frame (Habiband Schenk, 1999). Although the main objective for implementing a medium-format camera with airborne lidar is to produce orthophotos, stereo-overlapping images can derive digital height information as well. In favourable circumstances, a medium-format camera may also be used on its own for a survey project. This is the rationale behind this study. Compared with airborne lidar, digital aerial photographic surveying equipment is relatively lower in cost, its planimetric precision is higher and its height information can be derived more easily with automated matching. The high rate of image acquisition may provide high overlap percentages, which can be useful for increasing observations (Grenzdörffer, 2010).

In the context of marketing large-format digital cameras, several studies have evaluated the capability of the height determination of digital cameras (Haala et al., 2010). Höhle (2009) evaluated the heights obtained from automated matching usingZ/I Imaging's ImageStation® Automatic Elevations (ISAE) software. For images collected using the Vexcel UltraCam with an image scale of 1:6530 and an average flying height of 662 m, the standard deviation in height reached 0·13 m, which is equivalent to 0·02% of the flying height. The RMSE value was 0·14 m, which is equivalent to 0·022% of the flying height. Höhle (2009) documented the height accuracy obtained from a traditional film-based camera, a Zeiss RMK-TOP, with the image scale ranging from 1:3000 to 1:25 000. A standard deviation and RMSE of 0·011% and 0·019% of the flying height, respectively, were reported. The conclusion was that, in determining height, large-format digital cameras can reach approximately the same accuracy as traditional film-based metric cameras. However, relatively few studies have examined the performance of medium-format digital cameras. Hence, the current study explored the potential height accuracy of medium-format digital cameras.

Methodology

The objective of this research was to explore the capability of producing DEMs with medium-format camera images and direct georeferencing. In this study, the images captured with a medium-format camera in airborne lidar missions were used to produce a height

model by applying automated matching schemes. The height quality of the photogrammetrically produced data was compared with the DEM from lidar point clouds. Aerial triangulation with automated tie-point matching was applied to improve the geometric consistency between images; this was found to be crucial for better DEM matching. Note that because the acquisition of photography was not the primary task of the airborne lidar mission, the flights were not optimised for photogrammetric geometry.

The main tasks in this study involved pre-processing the data, generating the DEM and digital surface model (DSM), and analysing the data. The details of each step are given below.

Data Pre-processing

The data pre-processing step entails both lidar and photographic data. Lidar pre-processing is a standard procedure for meeting the requirements of DEM generation (Evans et al., 2009; USGS, 2010), and includes differential GPS, point cloud generation and strip adjustment. The trajectories of lidar systems are determined by using differential GPS. The distance between the working area and the GPS base station should be less than 30 km. The position, attitude and boresight calibration parameters are used to generate lidar point clouds. After the strip adjustment, the discrepancy between the strips is better than 0·15 cm in the overlap area.

The aim of photogrammetric image pre-processing is to obtain the interior and exterior orientation parameters for the images. Image pre-processing involves tie-point extraction and bundle adjustment. The adjusted GPS/inertial navigation system (INS) data provides initial orientation parameters for image matching in tie-point extraction. In this paper, Intergraph's ImageStation® Automatic Triangulation (ISAT) with an automated matching scheme was selected to refine the orientation parameters.

Lidar-Derived DEM

The airborne lidar data was post-processed using Terra Scan (Terrasolid, 2004) and followed the automated filtering scheme reported by Axelsson (2000), as well as the manual editing procedures. This filtering method entails using the terrain angle, iteration angle and iteration distance to select ground points automatically. The test area in this study was divided into different regions based on terrain complexity. After the automation process, an operator used shaded relief terrain and elevation profiles to edit the ground points. The automatic ground point selection works effectively in areas without vegetation. Because the lidar penetration rate in dense forests is relatively lower than in other areas, tree cover is a major issue when considering the quality of ground point selection; manual editing is required in such areas. After manual filtering, non-ground points were removed and the remaining points were treated as ground points. This study used the Points2Grid application (Crosby, 2010) to interpolate the ground points into the DEM. The interpolation methods of Points2Grid include minimum, maximum, mean and inverse distance weighting. The interpolation method used was the mean method: the mean elevation of the points within the predefined grid size was calculated and the calculated mean elevations were used to produce a DEM for each cell.

Photographically Derived DEM

Medium-format digital cameras enable the acquisition of highly overlapping images, which provide favourable geometrical configurations with high redundancy. The image-derived DEM can be produced by using two methods: the first is derived with automated

matching followed by filtering, and the other one is derived from manual stereo compilation. The choice between methods depends on the presence or absence of ground vegetation cover.

For the areas without vegetation, image matching alone was used to obtain the DEMs. The high similarity of adjacent stereo-images is beneficial for reliable automated image matching which was applied to generate 3D points for the medium-format images. This study used Inpho Match-T 5·2 (Inpho, 2009) for processing. Match-T does not perform multi-image matching simultaneously, but performs multiple pair-wise matching. Thus, each 3D point came from only one image pair. The DEM parameters were generation type, undulation terrain type, medium smoothing and feature density. These parameters were selected based on the characteristics of the test area.

For the vegetated area, an image-matching technique and manual stereo compilation were used to produce two DEMs. Because the height models derived from image matching are generally DSMs, they are not readily comparable with the DEM derived from lidar with manual editing. Manual stereo compilation, which involves following the standard operational procedure, was performed to digitise the contour lines in the stereo model. A grid DEM was generated with additional height points such as at peaks and troughs, as well as other independent points and constrained line data, such as breaklines, roads and the direct tracing of contours. Another editing scheme entails applying a filtering procedure for removing the effect of land cover.

Data Analysis

This study examined the accuracy and reliability of the elevation data derived from medium-format images. Because such images are acquired with lidar, this study used the lidar data as reference data. The following indices were used plus the median difference:

$$\text{Height difference, } \Delta h_i = h_{\text{photogrammetric}} - h_{\text{lidar}} \tag{1}$$

$$\text{Average difference, } \mu = \sum_i^n (\Delta h_i)/n \tag{2}$$

$$\text{Average absolute difference, } \mu' = \sum_i^n (|\Delta h_i|)/n \tag{3}$$

$$\text{Standard deviation, } \hat{\rho} = \sqrt{\left[\sum_i^n (\Delta h_i - \mu)^2\right]/(n-1)} \tag{4}$$

$$\text{Root mean square error, RMSE} = \sqrt{\left[\sum_i^n (\Delta h_i)^2\right]/n}. \tag{5}$$

First, all height differences between the photogrammetric and lidar data of the entire overlapped area were computed. This provided a general measurement of the total uncertainty. Subsequently, points located on flat areas without vegetation were selected to provide measurements independent from uncertainties introduced by both land cover and terrain slope. Points in the area of bare earth with various terrain slopes were subsequently evaluated. This

provided an opportunity to investigate the relationship between height uncertainty and terrain slope. Finally, the profiles of various types of land cover were obtained for visualising the relationship between height difference, land cover and terrain relief.

TEST DATA

The test site is located in Taichung County, Taiwan, comprising an area of approximately 8·7 km^2 along the Ta-An River. The landscape is mainly composed of a segment of the river channel and does not have heavy vegetation or many significant settlements. Roads and scattered buildings are present; however, the main land covers are grass, bushes, trees and bare earth. The purpose of the survey was to monitor the geomorphologic change of this area. Because of the geological uplift across the river induced by the Chi-Chi earthquake in 1999 and the ensuing river erosion, this area has attracted considerable research interest over the past 10 years. Routine mapping programmes have been established recently for this phenomenal geomorphic change, as well as for determining the potential risk to nearby structures. The orthophotos of the area are shown in Fig. 1. Table I lists the flying parameters of the two airborne lidar missions, which used a Leica ALS-50 scanner in June 2008 and an Optech ALTM 3070 in May 2009. The parameters of the medium-format Rollei AIC cameras used on the two flights (the 22-megapixel version in 2008 and the 39-megapixel version in 2009) are listed in Table II. In total, 28 photos were collected along one flight line in 2008, at an image scale of approximately 1/23 350; 151 photos were collected along five flight lines in 2009, at an image scale of approximately 1/18 330. The forward overlap averaged 68% in both cases. The equivalent ground resolution of each pixel was approximately 0·21 m for the images from 2008 and 0·13 m for those from 2009. The standard deviation for the bundle block adjustment for orientation determination

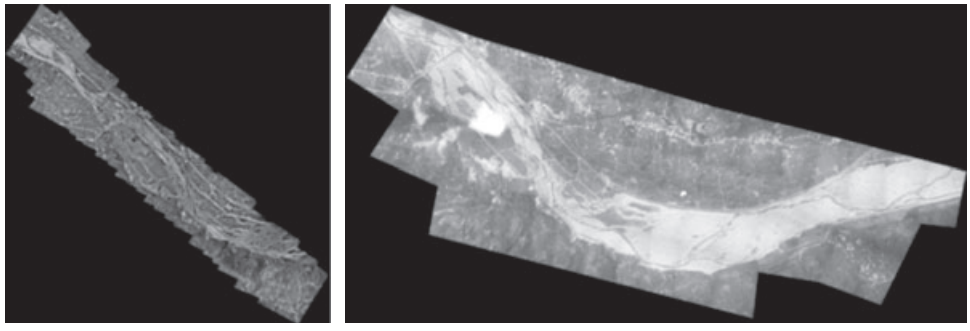

(a) Orthophotos in 2008 (b) Orthophotos in 2009

FIG. 1. Test area and location of aerial photos in the 2008 and 2009 flights. The test area in 2009 is larger than in 2008 and includes a mountainous area that was not part of the 2008 site.

TABLE I. Parameters of the airborne lidar.

	10th June 2008	*May 2009*
Scanner	Leica ALS-50	Optech ALTM 3070
Flying height above sea level	About 1650 m	About 1800 m
Flying height above ground	About 1209 m	About 1359 m
Laser repetition rate	65 200 Hz	70 000 Hz
Average point density	1·4 points/m^2	2·2 points/m^2

TABLE II. Parameters of the two Rollei AIC cameras.

Item	*10th June 2008*	*May 2009*
CCD chip	4080 × 5440 pixels	5415 × 7216 pixels
Image size	36·72 mm × 48·96 mm	36·80 mm × 49·07 mm
Principal distance (calibrated focal length)	51·780 mm	74·149 mm
CCD size	9 μm	6·8 μm

was approximately 1 pixel by using Intergraph's ISAT. The lens distortion of the Rollei AIC is relatively larger than that of a traditional large-format digital camera, which may have affected the bundle block adjustment result (Grenzdörffer, 2010). Furthermore, the accuracy of medium-format digital cameras is usually lower than that of their large-format cousins. Four sites were selected and analysed, as shown in Table III; the first "site" covers the entire area and Sites 1, 2 and 3 are smaller sites within this area.

To evaluate the height consistency between the lidar and photographic images, check points between the lidar point clouds and aerial stereo-images were manually measured using a digital photogrammetric system. The number of check points was 9 and 15 for 2008 and 2009, respectively. These check points were optimally distributed and were well-defined target-like symbols in the road. The mean error in the vertical direction for both cases was less than 10 cm. The standard errors in the vertical direction were 29 and 26 cm for 2008 and 2009, respectively.

EVALUATION

Assuming no error influences from the exterior and interior orientation parameters, the error propagation from the image-matching standard deviation σ_{mc} to the height σ_h can be determined by the following equation (Wolf and Dewitt, 2000):

$$\sigma_h = \sigma_{mc} \frac{H^2}{fB} \tag{6}$$

where H is the flying height above ground, f is the focal length and B is the base length between the two exposure stations.

For the June 2008 dataset, the average B/H ratio was 0·220. With a principal distance (calibrated focal length) of 51·78 mm and an average flying height above ground of 1209 m, the average theoretical height accuracy was ±0·97 m, assuming the matching accuracy was 1 pixel, which is 9 μm. In the July 2009 dataset, the average B/H ratio was 0·172. With a principal distance of 74·15 mm and an average flying height above ground of 1359 m, the

TABLE III. Different cases used for analysis.

Test site		*Description*
Entire area	Lidar	DSM: mixed land cover types
	Photographs	DSM: mixed land cover types
Site 1	Lidar	DSM: bare-earth area
	Photographs	DSM: bare-earth area
Sites 2 and 3	Lidar	DEM: vegetated; stereo compilation
	Photographs	DEM: vegetated; stereo compilation + automatic matching + filtering

average theoretical height accuracy was ±0·74 m, again assuming the matching accuracy was 1 pixel which is 6·8 μm for this data.

The nominal height accuracies from both the Leica ALS-50 and Optech ALTM 3070 were 0·15 m, because the GPS and INS data was received in favourable conditions. The analysis of lidar accuracies can be found in ASPRS (2004; 2005). Because the derived theoretical height accuracy from the medium-format camera imagery is approximately 1 m, the airborne lidar measurement can justifiably serve as the reference data for validating the photogrammetric surface.

With the topography being measured by lidar, the photogrammetric DEM and the height differences between the photogrammetric and lidar data are shown in Fig. 2 (for 2008) and Fig. 3 (for 2009). Fig. 2 shows the gridded DEM after mean interpolation. In order to reduce the effect of interpolation error, cells without points are assigned no value; the white dots shown in Fig. 2 were the cells without elevation data. Since the lidar point density is higher than the image-matching point density, the effect of white dots in the lidar DEM is less visible than with the photogrammetric DEM. The banding effect in Fig. 3 was also caused by the image-matching point density. Areas of high overlap have more observations during image matching and consequently produce more matched points than other areas. A bare-earth area

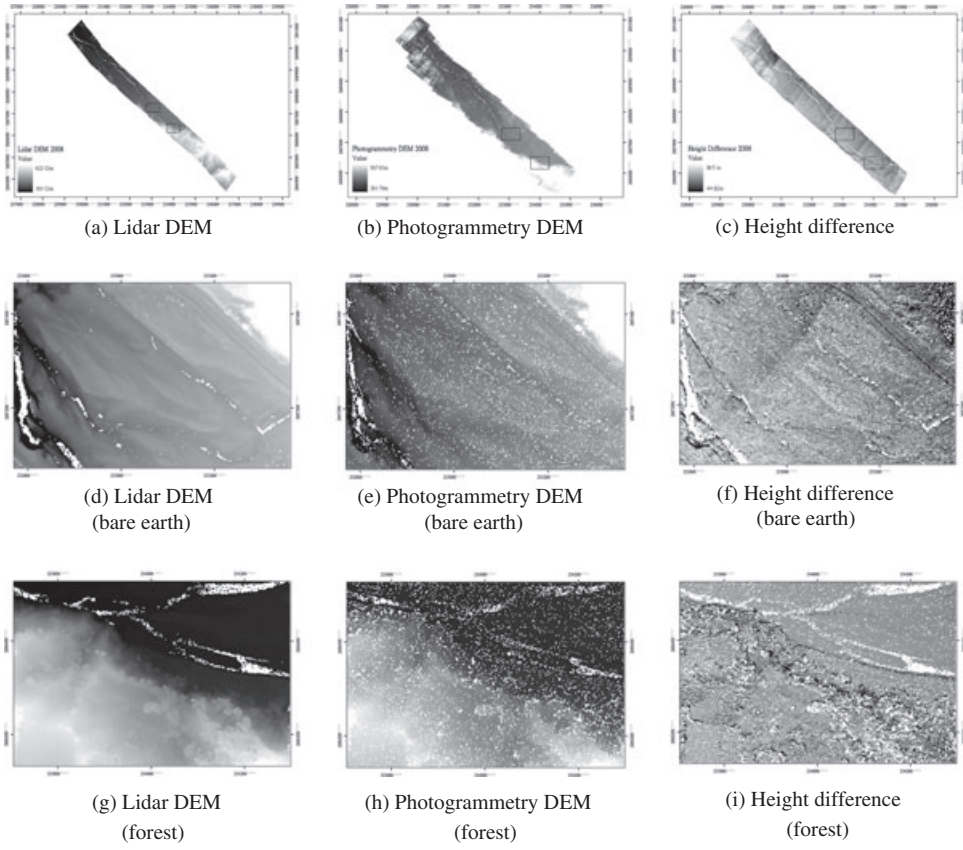

(a) Lidar DEM (b) Photogrammetry DEM (c) Height difference

(d) Lidar DEM (bare earth) (e) Photogrammetry DEM (bare earth) (f) Height difference (bare earth)

(g) Lidar DEM (forest) (h) Photogrammetry DEM (forest) (i) Height difference (forest)

FIG. 2. The terrain and height differences in 2008.

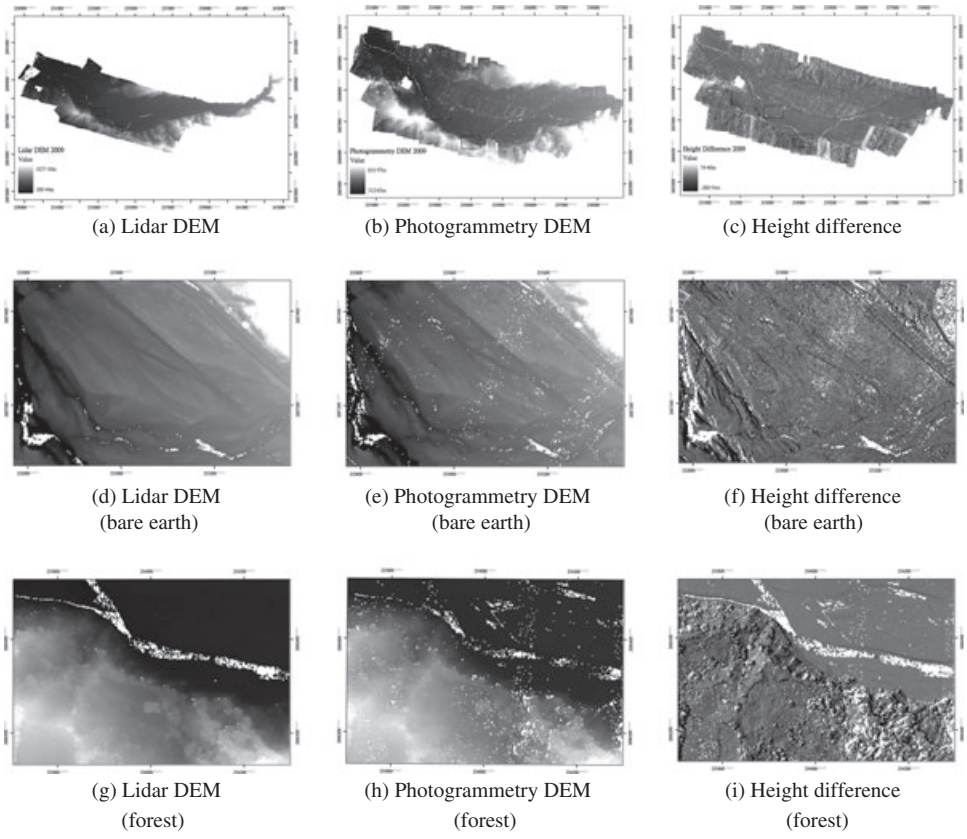

FIG. 3. The terrain and height differences in 2009.

and a forested area are also enlarged for comparison and shown in Figs. 2(d) to (i) and 3(d) to (i). For comparison purposes, note that the height differences in the bare-earth area are smaller than those in the forested area and, consequently, the height differences are not the absolute errors but are the differences between the two approaches. Large errors occurred towards the periphery because matching errors frequently occurred near the edge of the photographs. The standard deviation of the height difference and other indices are presented in Table IV. Because the entire test area in 2009 includes a mountainous region which was beyond the limits of the 2008 site, it is more complicated than the one imaged in 2008. Hence, the RMSE in 2009 is less favourable than that in 2008. The height difference in this study was larger than

TABLE IV. Error indices of the entire area.

Items	*2008*	*2009*
Number of points	1 306 108	4 830 659
Average difference (m)	0·24	−0·45
Median difference (m)	0·31	−0·30
Average absolute difference (m)	1·06	1·08
Standard deviation (m)	1·68	2·08
RMSE (m)	1·69	2·13

the theoretical value because land cover types such as vegetation and buildings induced large height differences. To avoid the influence of such problematic land cover types, the evaluation was performed for the bare-earth area only. In addition to the vegetation concern, the horizontal positioning accuracy may have contributed an error to the height evaluation.

Relationship between Slope and Height Difference

To investigate the effect of slope on height differences, only bare-earth areas were used. Two evaluations were undertaken: the first used only flat bare-earth check points distributed over the entire area; the second used bare sloping areas in Site 1. In the first evaluation, only points located in relatively flat areas with slopes lower than 5°, such as on most roads, were included. These points were selected over the entire area. The locations of 90 flat bare-earth reference points are shown in Fig. 4; these were selected from the lidar data and most of them are located on road surfaces. In the image space, a road is usually a homogenous area without features for image matching. Hence, some reference points are missing in the photogrammetric DEM. Other points do not have height values in either the lidar or photogrammetric DEMs. Hence, there are 78 check points for 2008 and 85 check points for 2009. For validation purposes, this study selected the total height error computed as the differences among the check point heights. The second evaluation was again limited to the bare-earth areas; however, results from various terrain slopes in Site 1 were analysed.

The height standard deviations for 2008 and 2009 were 0·62 and 0·27 m, respectively (Table V), which means the consistency between the lidar and medium-format photography is better in 2009 than in 2008. The RMSE was 0·65 m for 2008 and 0·37 m for 2009. The differences of 97% of the samples were less than $\pm 1{\cdot}25$ m. The average height determined by photogrammetry was 0·20 m higher than that from lidar for the 2008 dataset, but 0·25 m lower than lidar for 2009. Although this is relatively insignificant considering the 0·62 and 0·27 m standard deviation figures, and the 0·15 m nominal height accuracy of lidar, the trend is remarkable. Compared with the theoretical error estimate, the matching accuracy reached a sub-pixel level. Based on a detailed examination of the ground control points, the tie points generated by the matching algorithm in the automated aerial triangulation procedure

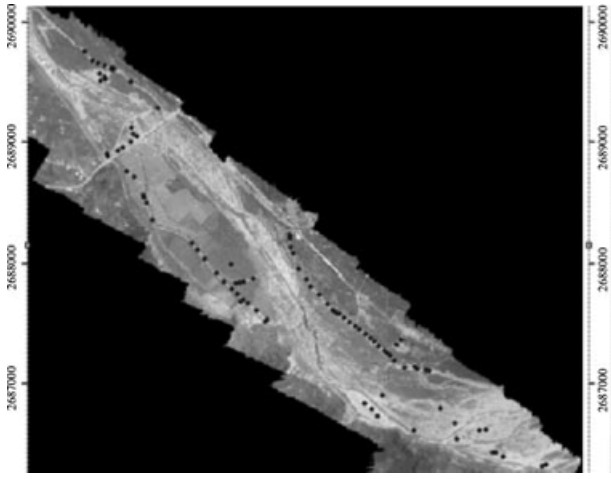

FIG. 4. Location of the 90 flat bare-earth reference points (shown as dots).

TABLE V. Error indices of points located in flat bare-earth area.

Indices	*2008*	*2009*
Number of points	78	85
Average difference (m)	0·20	−0·25
Median difference (m)	0·29	−0·25
Average absolute difference (m)	0·53	0·30
Maximum difference (m)	1·56	0·52
Minimum difference (m)	−3·23	−1·60
Standard deviation (m)	0·62	0·27
RMSE (m)	0·65	0·37

are most likely to be the major source of uncertainty, due to the lack of well-defined targets in the scene, which is mainly a vegetated area along a river bank with bare areas only immediately adjacent to the river.

The differences between the results from 2008 and 2009 can be attributed to several factors. First, the geometrical configuration of 2009 is more favourable than that of 2008; the data taken in 2008 involves only one strip (28 photos), where as the data taken in 2009 uses three overlapped strips (151 photos). Second, the image scale for the 2009 flight is larger (1/18 330, compared with 1/23 350 in 2008). Third, the field of view for the 2008 photography is larger than that in 2009, which means the effect of lens distortion for the 2008 data is larger than for the 2009 photography.

Site 1 was a large bare-earth area covered by 25 309 pixels in 2008 and 26 232 pixels in 2009. The total area is 12·1 ha, characterised by a large range of slopes, from 0 to 90° (Fig. 5). The ground materials are mainly sands, gravels of various sizes, sandstone and soil. In the 2008 dataset the height of this area ranged from 358 to 394 m, the height difference ranged from −14 to 18 m and the slopes ranged from 0 to 80° (Fig. 6(a) to (c)). In 2009, the heights ranged from 353 to 389 m, the height difference ranged from −26 to 15 m and the slopes again ranged from 0 to 80° (Fig. 6(d) to (f)). The error indices for the sloping bare-earth Site 1 test area are tabulated in Table VI. As expected, a clear trend was observed of the RMSE increasing with the slope (Fig. 7). Toutin (2006) reported similar results on DSMs generated

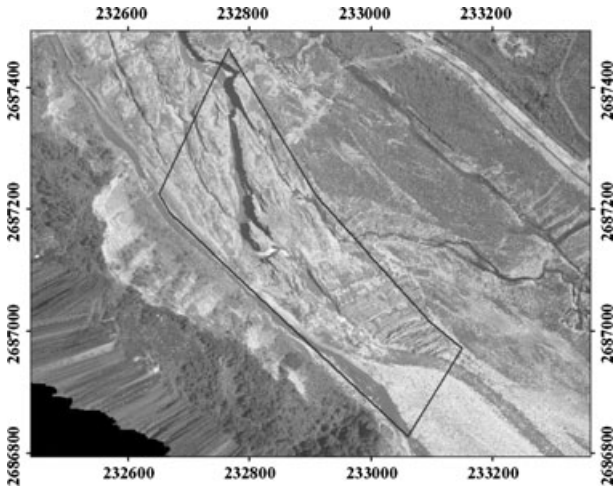

FIG. 5. Orthophoto of the sloping bare-earth test area. Site 1 is indicated by the black line.

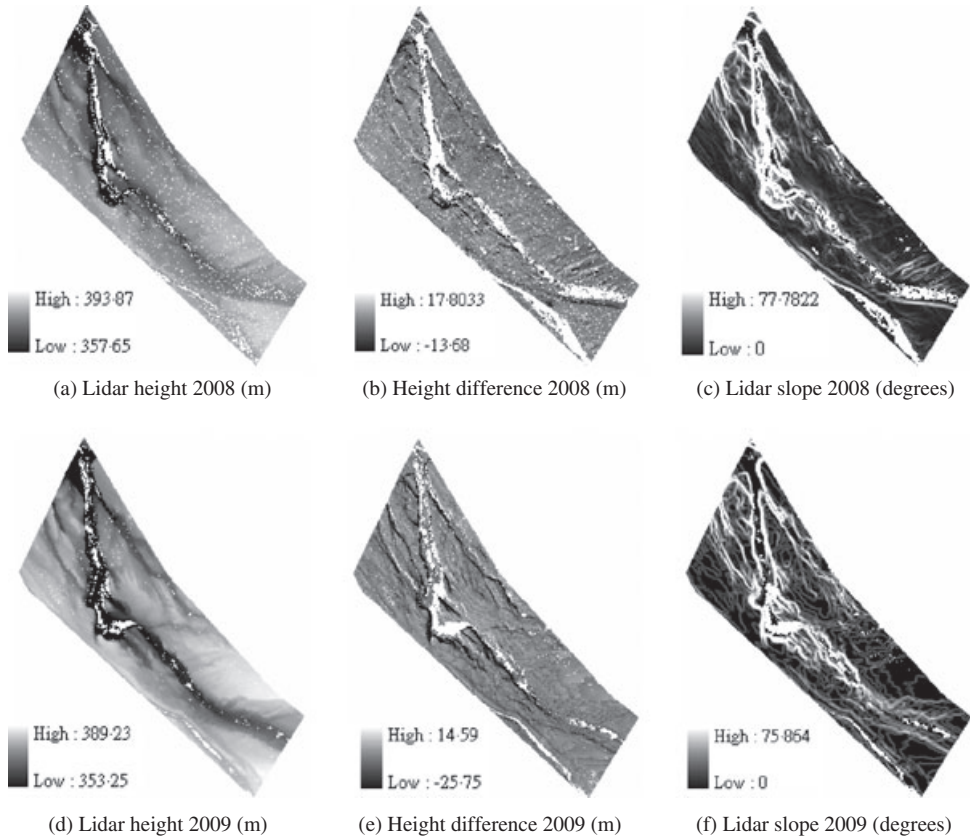

(a) Lidar height 2008 (m) (b) Height difference 2008 (m) (c) Lidar slope 2008 (degrees)

(d) Lidar height 2009 (m) (e) Height difference 2009 (m) (f) Lidar slope 2009 (degrees)

FIG. 6. Site 1 bare-earth test areas in 2008 and 2009.

TABLE VI. The error indices of the sloping bare-earth area of Site 1.

Indices	*2008*	*2009*
Number of points	24 053	26 232
Average difference (m)	1·04	−0·23
Median difference (m)	1·13	−0·06
Average absolute difference (m)	1·18	0·70
Maximum difference (m)	17·80	14·59
Minimum difference (m)	−13·68	−25·75
Standard deviation (m)	0·95	1·35
RMSE (m)	1·41	1·37

from satellite images and lidar DSMs, and indicated that when the terrain slope is less than 20°, there is a linear relationship between the elevation error and the terrain slope.

The RMSEs of the bare-earth areas (Table VI) were considerably smaller than that of the entire area (Table IV). The photogrammetric surface was substantially higher than that of the lidar measured for 2008, and lower than the lidar measured for 2009. This is particularly evident when comparing the average difference and average absolute difference.

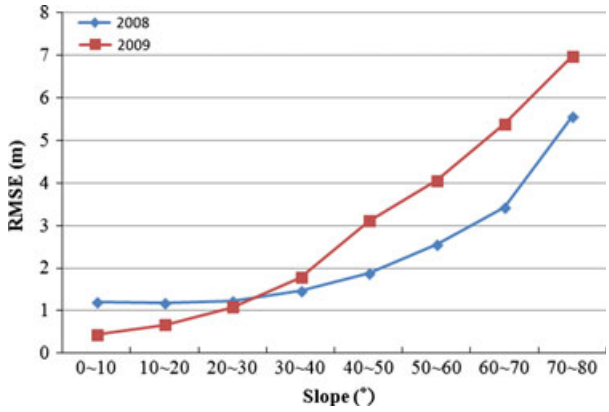

FIG. 7. RMSE of height difference sampled with slope increments of 10° for Site 1. Small triangles represent 2008 data; larger squares represent 2009 data.

Although the slope is a common factor in height accuracy assessment, the relationship between the degree of slope and the RMSE was further examined using various slope increments.

Profile Analysis

Eight profiles were selected for profile analysis (Fig. 8). Profiles p1 to p4 are located in the bare-earth area of Site 1 and the profiles are shown in Fig. 9. Profiles q1 and q2 are located in a vegetated part in the north-west of the entire area; q3 and q4 are again vegetated but to the south-east; the corresponding profiles are shown in Fig. 10.

As far as the bare-earth profiles (p1 to p4) are concerned, an offset between the lidar and photogrammetry was observed from the 2008 profile p1 in Fig. 9(a). This systematic difference might result from the uncertainties in image orientation. Moreover, the height distribution of the lidar DEM of 2008 is relatively smooth compared to that of the photogrammetric DEM. The profile in 2009 is generally more consistent. A similar phenomenon is shown in Fig. 9(b), where a spike in the 2008 photogrammetric profile of p2 may be the result of a matching error located at 120 m. Fig. 9(c) shows a larger deviation in profile p3 between 2008 and 2009 occurring in the interval 0 to 50 m, whereas the remainder of the profile is more consistent. Fig. 9(d) shows that a large error occurred in the interval of 0 to 50 m, and at a profile distance of 80 m there is a building that was missed in the 2008 photogrammetric DEM. In 2009, the photogrammetric DEM height distribution exhibited a clear trend in that a building was present. The profile reveals that a larger height error and offsets occurred in the steep slope area. The planar resolution influences the height accuracy, which is magnified depending on the steepness of the slope.

Fig. 10 compares lidar and photogrammetric profiles (q1 to q4) in two vegetated areas. The trends of both surfaces are very similar. Only some tops of tree crowns are different.

Comparison between Manual and Automatic Image-Derived DEM

Two image-derived DEMs were generated in the vegetated areas. The first is a manually-edited DEM and the second is an automatically-matched DEM. Both image-

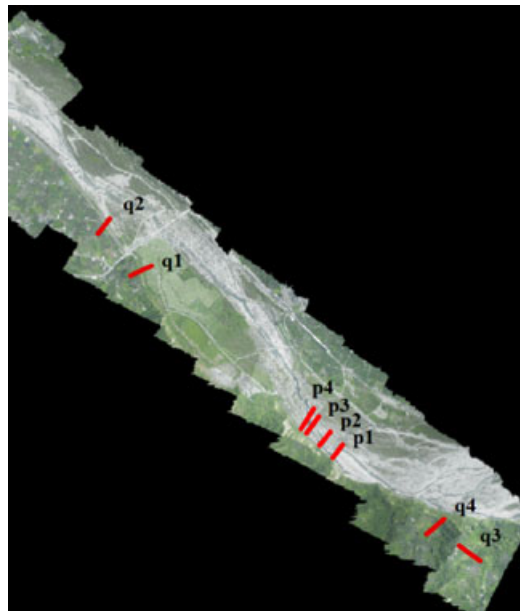

(a) General location of the eight profiles.

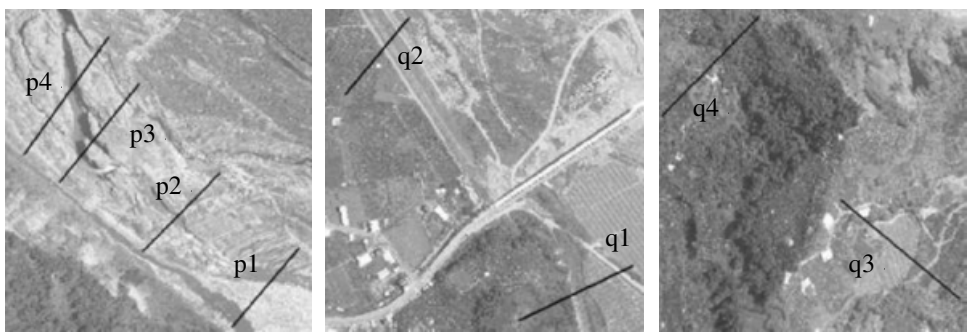

(b) Bare earth (c) Vegetated (d) Vegetated

FIG. 8. The eight profiles. (a) General location of profiles. (b) p1 to p4 are in bare-earth areas of Site 1. (c), (d) q1 to q4 are in two vegetated regions of the entire area.

derived DEMs were compared by using the lidar-derived DEM. The aim of this part of the study was to analyse the effect of vegetation.

Two test vegetated areas, Sites 2 and 3, were selected for examining DEM production with human stereo compilation. Site 2 has an area of 18·3 ha and Site 3 covers 16·7 ha. As shown in Fig. 11, Site 2 had considerable vegetative cover. A number of vegetated areas and buildings were present in Site 3 (Fig. 12). The height differences are shown in Figs. 11(e), (f) and 12(e), (f). For Site 2, the height difference ranged from −17 to +10 m when using stereo compilation and −11 to +16 m using auto-matching with filtering. The densely vegetated cover is one of the crucial factors that influence the filtering results. For Site 3, the height differences are −9 to +6 m by performing stereo compilation and −5 to +14 m by using

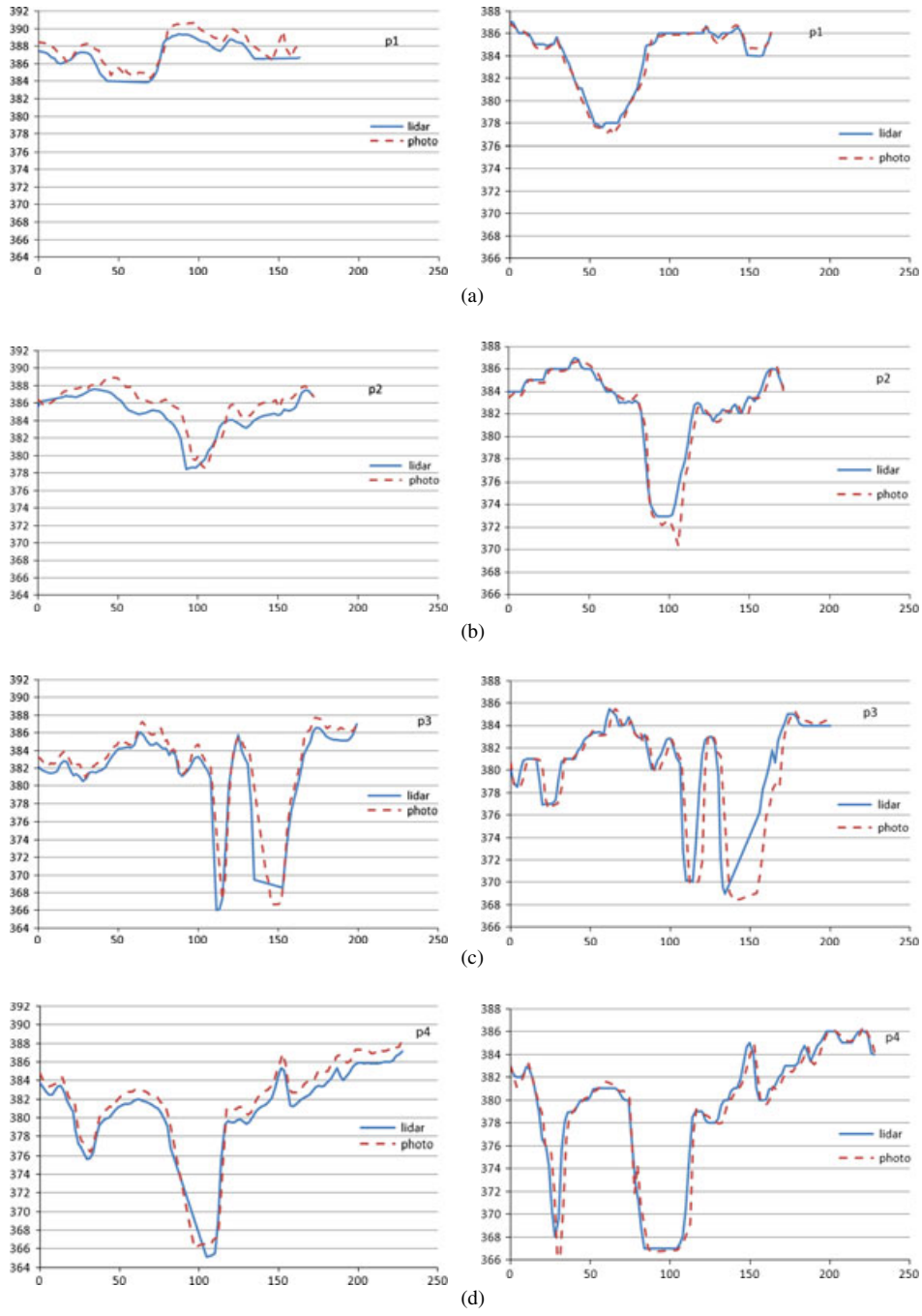

FIG. 9. Profiles p1 to p4 of bare-earth areas in 2008 (left) and 2009 (right) (metres). Solid lines represent the lidar DEM; pecked lines represent the photogrammetric DEM.

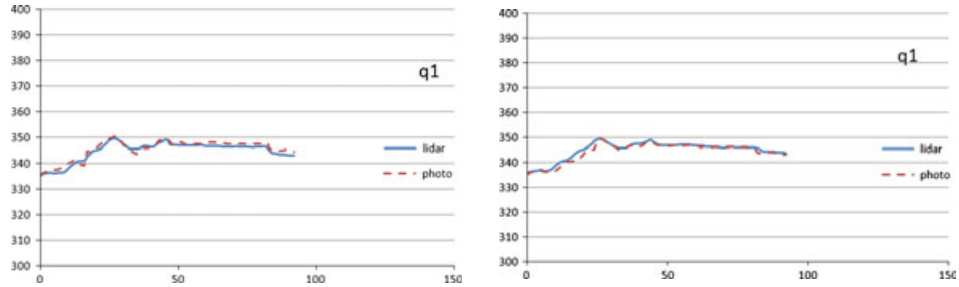

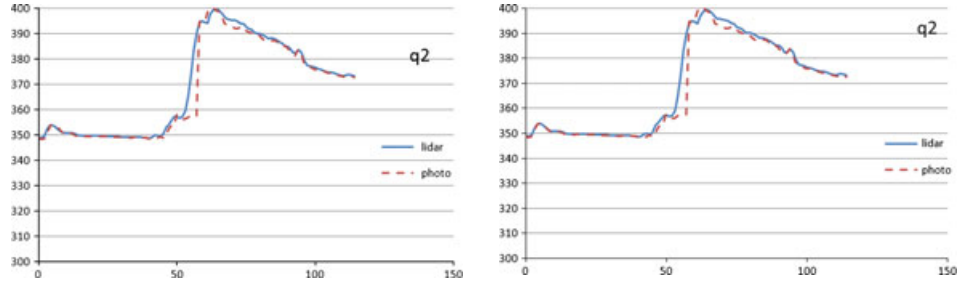

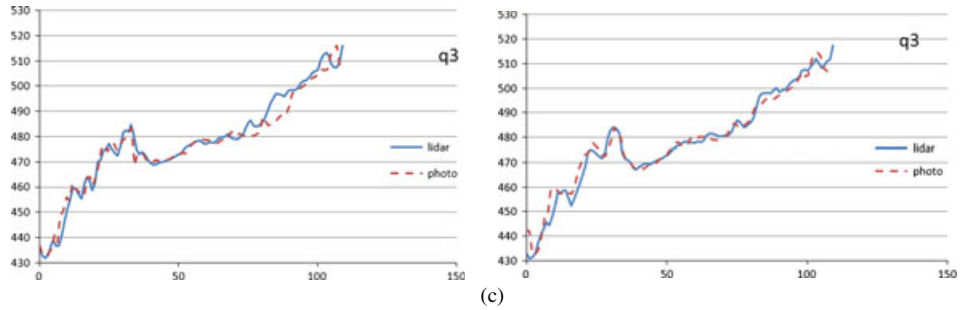

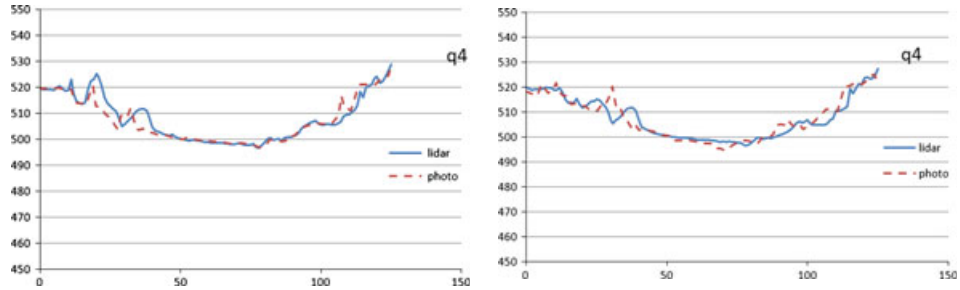

FIG. 10. Profiles q1 to q4 of two vegetated areas in 2008 (left) and 2009 (right) (metres). Solid lines represent the lidar DEM; pecked lines represent the photogrammetric DEM.

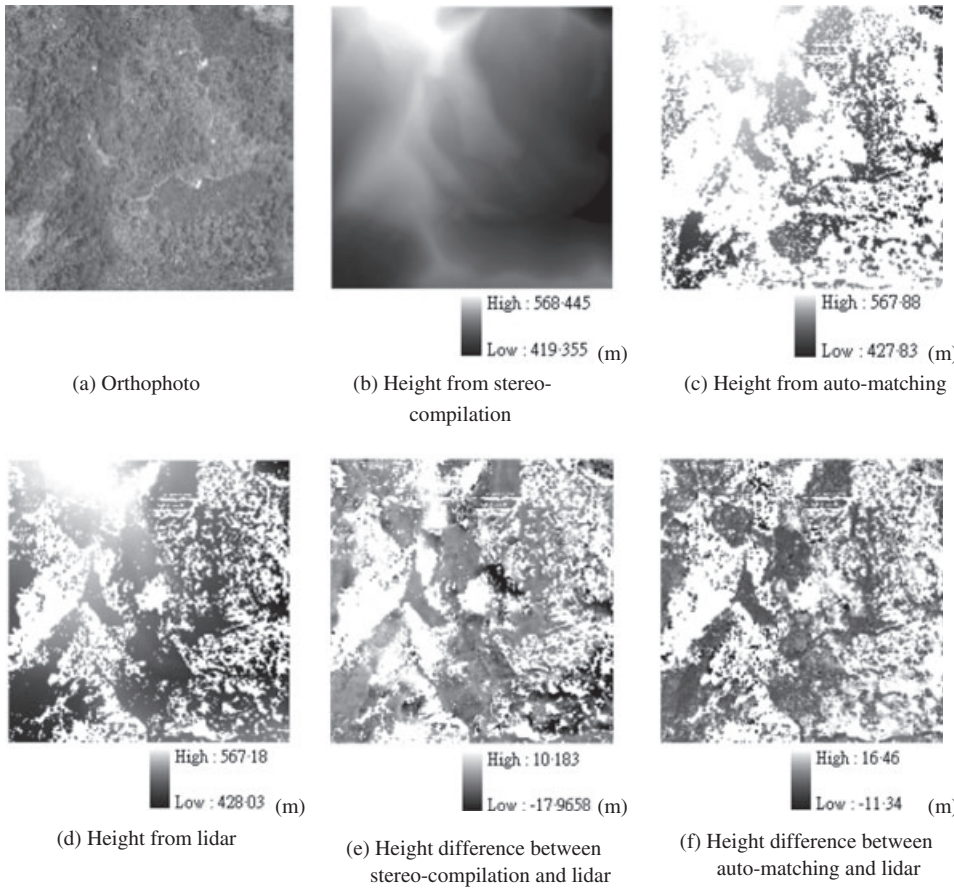

(a) Orthophoto

(b) Height from stereo-compilation

(c) Height from auto-matching

(d) Height from lidar

(e) Height difference between stereo-compilation and lidar

(f) Height difference between auto-matching and lidar

FIG. 11. Site 2. All figures in metres.

filtering. The error indices for Sites 2 and 3 are listed in Tables VII and VIII. For Site 2, 58% of height differences derived from stereo compilation was smaller than 1 m; for auto-matching and filtering the figure was 72%. The equivalent percentages for Site 3 are 88% and 71%, respectively. The RMSE of Site 2 derived from stereo compilation was notably larger than that derived from auto-matching with filtering, whereas the converse was observed for Site 3. This was likely to have been caused by difficulties in stereo compilation, in which the true surface is identified by human conjecture. The vegetation and the steep slope may be crucial factors that influence the process of human editing.

Fig. 13 shows the dependency of height difference on slope angle. Note the large deviation which is apparent for slopes above 60°. The RMSE of manual editing is larger than that of auto-matching when the slope is larger than 60°. This indicates that manual editing created larger uncertainties in the densely vegetated area.

Whereas the matching accuracy reached the sub-pixel level for the flat bare-earth area, the height deviation in the vegetated area was larger than the theoretical value. The RMSEs of the two bare-earth test areas were considerably smaller than that of the entire area.

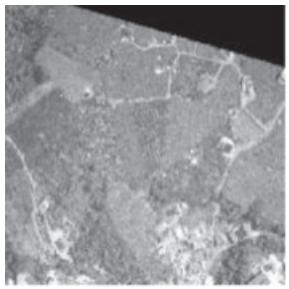

(a) Orthophoto

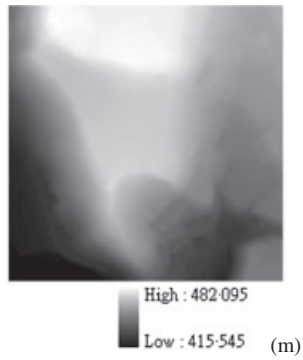

(b) Height from stereo-compilation

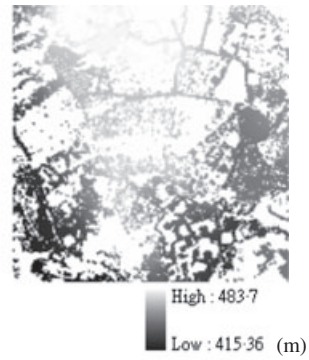

(c) Height from auto-matching

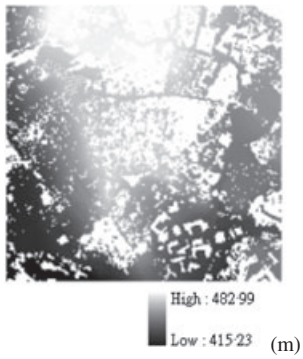

(d) Height from lidar

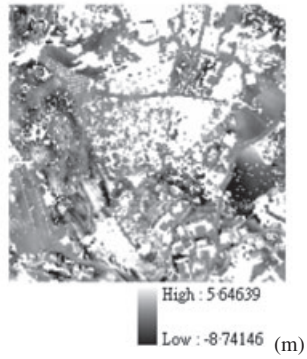

(e) Height difference between stereo-compilation and lidar

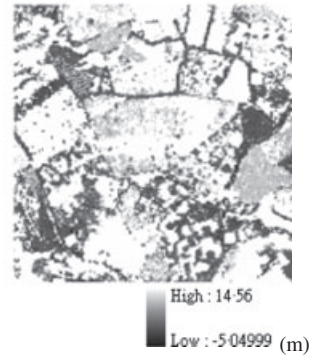

(f) Height difference between auto-matching and lidar

FIG. 12. Site 3. All figures in metres.

TABLE VII. The error indices of DEM test area.

	Site 2 Manual	*Site 3 Manual*	*Site 2 Auto-matching*	*Site 3 Auto-matching*
Number of points	23 395	25 790	11 608	16 760
Average difference (m)	−0·28	−0·11	0·77	0·40
Median difference (m)	−0·04	−0·02	0·40	0·05
Average absolute difference (m)	1·34	0·48	0·99	0·68
Maximum difference (m)	10·18	5·65	16·46	14·56
Minimum difference (m)	−17·97	−8·74	−11·34	−5·05
Standard deviation (m)	2·10	0·73	1·63	0·97
RMSE (m)	2·12	0·74	1·80	1·04

TABLE VIII. The height difference magnitude distribution.

Height difference	*Site 2 Manual*	*Site 3 Manual*	*Site 2 Auto-matching*	*Site 3 Auto-matching*
0 to 0·5 m	8071 (34%)	17 852 (69%)	5748 (50%)	9906 (59%)
0·5 to 1 m	5515 (24%)	4817 (19%)	2523 (22%)	1974 (12%)
1 to 2 m	5221 (22%)	2503 (10%)	1962 (17%)	4350 (26%)
2 to 3 m	1996 (9%)	451(2%)	645 (5%)	406 (2%)
>3 m	2592 (11%)	167 (0%)	730 (6%)	124 (1%)

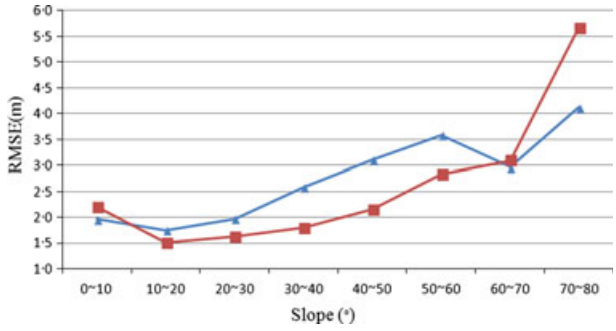

Site 2

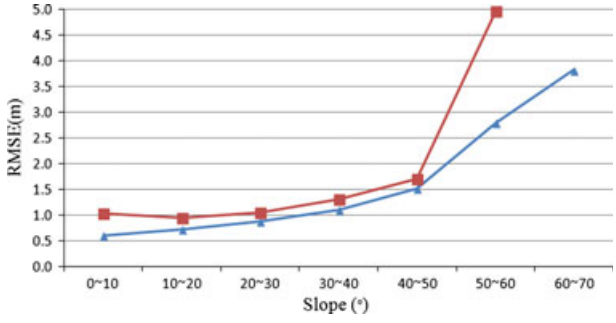

Site 3

FIG. 13. The RMSE of height difference sampled with slopes at 10° increments. Small triangles represent manual editing. Large squares represent auto-matching.

CONCLUSION

Medium-format digital cameras are used in several applications, one of which involves generating elevation data from stereo-images. This study analysed the quality of digital elevation data derived from a medium-format camera using lidar data. The height accuracy from medium-format cameras was evaluated using a lidar-derived DSM and DEM as the reference data. Using a multiple image-matching method to generate the DSM, subsequent automatic and manual filtering methods were applied to produce the DEM. Two test areas

with various land cover types were included in the experiment. The research has shown that medium-format cameras have the potential to produce meaningful DEMs in flat, bare-earth areas such as Site 1. However, the results deteriorate as the slope increases, and the presence of vegetation causes major uncertainties in the DEM data.

The influence of planar resolution was demonstrated in the profiles, especially in the steeply sloping area. The results from analysing the removal of land cover indicate that the DEM derived from manual stereo compilation has a similar RMSE to that for the entire area. At Site 2, auto-matching with filtering was superior to stereo compilation, because the large proportion of vegetation covering the area increasingly hindered human judgment, which subsequently led to a large error. Site 3 had less vegetative cover and a superior height accuracy for stereo compilation.

ACKNOWLEDGEMENTS

The authors are grateful to the anonymous reviewers for valuable comments and suggestions which greatly improved the paper. The authors also wish to thank the National Science Council, Taiwan, Republic of China, for financially supporting this project through grant NSC 101-2625-M-009-011.

REFERENCES

ASPRS, 2004. ASPRS guidelines: vertical accuracy reporting for lidar data.http://www.asprs.org/a/society/committees/standards/Vertical_Accuracy_Reporting_for_Lidar_Data.pdf [Accessed: 12th January 2012].

ASPRS, 2005. ASPRS lidar guidelines: horizontal accuracy reporting.http://www.asprs.org/a/society/committees/standards/Horizontal_Accuracy_Reporting_for_Lidar_Data.pdf [Accessed: 12th January 2012].

AXELSSON, P., 2000. DEM generation from laser scanner data using adaptive TIN models.*International Archives of Photogrammetry, Remote Sensing and Spatial Information Sciences*, 33(B4): 110–117.

BALTSAVIAS, E. P., 1999. A comparison between photogrammetry and laser scanning. *ISPRS Journal of Photogrammetry and Remote Sensing*, 54(2/3): 83–94.

BROWN, D. C., 1966. Decentering distortion of lenses. *Photogrammetric Engineering*, 32(3): 444–462.

CROSBY, C., 2010. GEON Points2Grid utility instructions.Arizona State UniversityActive Tectonics Research Group, Arizona, USA. http://lidar.asu.edu/downloads/GEON_Points2Grid_Instructions.pdf [Accessed: 19th August 2011].

EVANS, J. S., HUDAK, A. T., FAUX, R. and SMITH, A. M. S., 2009. Discrete return lidar in natural resources: recommendations for project planning, data processing, and deliverables. *Remote Sensing*, 1(4): 776–794.

GRENZDÖRFFER, G., 2010. Performance of medium format digital airborne cameras. *EuroSDR Official. Publication*, 58: 233–265.

HAALA, N., HASTEDT, H., WOLF, K., RESSL, C. and BALTRUSCH, S., 2010. Digital photogrammetric camera evaluation – generation of digital elevation models. *Photogrammetrie. Fernerkundung, Geoinformation*, 2010–2: 99–115.

HABIB, A. and SCHENK, T., 1999. A new approach for matching surfaces from laser scanners and optical sensors. *International Archives of Photogrammetry and Remote Sensing*, 14(3/W14): 55–61.

HABIB, A. and MORGAN, M., 2005. Stability analysis and geometric calibration of off-the-shelf digital cameras. *Photogrammetric Engineering & Remote Sensing*, 71(6): 733–741.

HABIB, A., JARVIS, A., QUACKENBUSH, P. and STENSAAS, G., 2007. Medium-format digital cameras: a study into the calibration, stability analysis, and achievable accuracy.*ASPRS 2007 Annual Conference*, Tampa, Florida, USA.12 pages.

HÖHLE, J., 2009. DEM generation using a digital large format frame camera. *Photogrammetric Engineering & Remote Sensing*, 75(1): 87–93.

HÖHLE, J., 2013. Assessing the positional accuracy of airborne laser scanning in urban areas. *Photogrammetric Record*, 28(142): 196–210.

INPHO, 2009. Match-T DSM Reference Manual. *Inpho*. 182 pages.

PETRIE, G. and WALKER, A. S., 2007. Airborne digital imaging technology: a new overview. *Photogrammetric Record*, 22(119): 203–225.

RIEKE-ZAPP, D. H., 2010. A digital medium-format camera for metric applications –Alpa 12 Metric. *Photogrammetric Record*, 25(131): 283–298.
TERRASOLID, 2004. *TerraScan User's Guide* (18th November 2004). *Terrasolid.* 308 pages.
TOUTIN, T., 2006. Generation of DSMs from SPOT-5 in-track HRS and across-track HRG stereo data using spatiotriangulation and autocalibration. *ISPRS Journal of Photogrammetry and Remote Sensing*, 60(3): 170–181.
USGS, 2010. Lidar guidelines and base specification, Version 13.http://lidar.cr.usgs.gov/USGS-NGP%20Lidar%20Guidelines%20and%20Base%20Specification%20v13(ILMF).pdf [Accessed: 12th January 2012].
WOLF, P. R. and DEWITT, B. A., 2000. *Elements of Photogrammetry with Applications in GIS*. Third edition. McGraw-Hill, New York, USA. 608 pages.

Résumé

Les appareils photo numériques moyen format sont appropriés pour la production d'ortho-images lors de missions lidar aéroportées. Cette étude s'intéresse à la qualité des MNE (modèles numériques d'élévation) et MNS (modèles numériques de surface) obtenus à partir de tels instruments. Une stratégie d'appariement d'images est mise en œuvre pour produire une information altimétrique à partir d'images à fort recouvrement et la qualité de l'altitude obtenue est analysée en utilisant les nuages de points lidar comme des données de référence. L'évaluation porte sur plusieurs types d'occupation du sol et plusieurs méthodes de production de MNE. Les erreurs moyennes quadratiques obtenues, pour deux jeux de données, entre les altitudes issues du lidar et des images, sont de 0·054% et 0·027% de la hauteur de vol sur des zones plates et dégagées, mais des études conduites manuellement en utilisant des données de stéréophotogrammétrie sur des zones couvertes de végétation mettent en évidence des incertitudes élevées, notamment en présence de fortes pentes.

Zusammenfassung

Mittelformatige Digitalkameras werden bei flugzeuggestütztem Laserscanning (LIDAR) zur Produktion digitaler Orthophotos eingesetzt. In dieser Studie wird die Qualität von Digitalen Höhenmodellen (engl. DEMs) und Digitalen Oberflächenmodellen (engl. DSMs), die aus solchen Kameras abgeleitet werden untersucht. Eine Bildzuordnungsstrategie zur Ableitung von Höheninformation aus stark überlappenden Bildern wird mit Hilfe eines Referenzdatensatzes aus synchron aufgenommenen LIDAR-Punktwolken analysiert. Die Analyse umfasste dabei verschiedene Landschaftstypen und Methoden zur Produktion digitaler Höhenmodelle. Der RMSE Wert zwischen LIDAR-Punktwolken und Punktwolken aus Bildzuordnung zweier Datensätze lag bei 0·054% bzw. 0·027% der Flughöhe in flachen Gebieten ohne Bewuchs. Studien mit manuell editierten bewachsenen Gebieten legten jedoch hohe Messunsicherheiten, speziell in steilem Gelände, offen.

Resumen

Las cámaras digitales de medio formato son herramientas útiles para producir ortoimágenes en vuelos lidar. En este estudio se investiga la calidad de modelos de elevación digitales (MEDs) y de modelos de superficie (MDSs) derivados de estas cámaras. La altura se determina mediante técnicas de correspondencia de imágenes, las cuales tienen un gran recubrimiento. Su calidad se determina usando nubes de puntos lidar simultáneos como referencia. La evaluación se centra en los distintas cubiertas del suelo y los métodos de generación de MEDs. El error RMS entre las alturas lidar y las derivadas de las imágenes en dos conjuntos de datos es de 0·054% y 0·027% de la altura de vuelo en terreno llano y descubierto. Estudios con edición estereoscópica manual en áreas con vegetación muestran grandes incertidumbres, especialmente en zonas con pendiente.